



Volume 57 Number 4 April 2019  
ISSN 0042-3114

Vehicle  
System  
Dynamics

International Journal  
of Vehicle Mechanics  
and Mobility

Official Organ of the  
Editor

International Association  
for Vehicle System  
Dynamics  
Motoo Aoyanagi  
Shirokatsu Horuchi  
Satoru Iwaki  
Masafumi Iwase

Taylor & Francis  
Taylor & Francis Group

# Vehicle System Dynamics

## International Journal of Vehicle Mechanics and Mobility

ISSN: 0042-3114 (Print) 1744-5159 (Online) Journal homepage: <https://www.tandfonline.com/loi/nvsd20>

## Robust road friction estimation during vehicle steering

Liang Shao, Chi Jin, Cornelia Lex & Arno Eichberger

To cite this article: Liang Shao, Chi Jin, Cornelia Lex & Arno Eichberger (2019) Robust road friction estimation during vehicle steering, Vehicle System Dynamics, 57:4, 493-519, DOI: [10.1080/00423114.2018.1475678](https://doi.org/10.1080/00423114.2018.1475678)

To link to this article: <https://doi.org/10.1080/00423114.2018.1475678>



Published online: 22 May 2018.



Submit your article to this journal 



Article views: 268



View Crossmark data 



## Robust road friction estimation during vehicle steering

Liang Shao<sup>a</sup>, Chi Jin<sup>b</sup>, Cornelia Lex<sup>a</sup> and Arno Eichberger<sup>a</sup>

<sup>a</sup>Institut für Fahrzeugtechnik, Technische Universität Graz, Graz, Austria; <sup>b</sup>Laboratoire des Signaux et Systèmes (L2S), CentraleSupélec-CNRS-Université Paris Sud, Gif-sur-Yvette, France

### ABSTRACT

Automated vehicles require information on the current road condition, i.e. the tyre-road friction coefficient for trajectory planning, braking or steering interventions. In this work, we propose a framework to estimate the road friction coefficient with stability and robustness guarantee using total aligning torque in vehicle front axle during steering. We first adopt a novel strategy to estimate the front axle lateral force which performs better than the classical unknown input observer. Then, combined with an indirect measurement based on estimated total aligning torque and front axle lateral force, a non-linear adaptive observer is designed to estimate road friction coefficient with stability guarantee. To increase the robustness of the estimation result, criteria are proposed to decide when to update the estimated road conditions. Simulations and experiments under various road conditions validate the proposed framework and demonstrate its advantage in stability by comparing it with the method utilising the wide-spread Extended Kalman Filter.

### ARTICLE HISTORY

Received 11 October 2017

Revised 5 February 2018

Accepted 22 April 2018

### KEYWORDS

Road friction estimation;  
active safety; adaptive  
observer; automated driving

## 1. Introduction

Many traffic-safety related investigations demonstrate a correlation between the road condition and accidents probability [1]. With development of highly automated and autonomous vehicles, the responsibility to adapt the driving style like braking and steering to the road condition is transferred from the driver to the automated systems. Therefore, regarding vehicle safety and performance, road friction coefficient  $\mu_{\max}$  estimation is more critical for designing planning and control systems, such as trajectory planning [2] and path tracking [3].

Real-time approaches to determining  $\mu_{\max}$  during driving can be mainly classified as cause-based methods and effect-based methods [4]. By using vision, laser, temperature or other sensors [5–8], cause-based methods detect materials covering road surfaces, such as water, ice and snow, in this way the road condition in front of the car can be estimated. However, these methods often require additional sensors installed on series production vehicles. Besides, only an interval of road friction coefficient can be obtained which can be quite large sometimes, for example, on wet road condition, the interval may vary from 0.3 to 0.9 [9]. Effect-based methods measure parameters influenced by the road condition,

**CONTACT** Liang Shao liang.shao@tugraz.at

for example, tyre tread deformation [10,11], acoustic [12–14], slip–slope relationship in longitudinal directions [15–17], vehicle lateral dynamics without [18–20] or with total aligning torque information [21–25]. Mostly, these effect-based methods only utilise the sensor information on the series production vehicles which is a pro, but adequate excitation is necessary for the road friction coefficient estimation. Therefore, there are also some research combining cause-based methods and effect-based methods to better obtain road conditions [26,27].

In this article, an effect-based method is presented which utilises vehicle lateral dynamics related information. With this approach, predicting  $\mu_{\max}$  ahead of the vehicle is not possible and it cannot offer an accurate value of  $\mu_{\max}$  to a vehicle control system before a certain excitation level is reached [28]. But with sufficient excitation, it is possible to get a more accurate estimate rather than, e.g. a range like with optical sensors. The effect-based method presented in this article may be one part of a future road condition strategy in combination with optical or infrastructural data. At times when the excitation is not sufficient, which will often be the case, e.g. during the trajectory planning process, other data will be used to get a rough estimate of the road condition. Once the excitation is sufficient, e.g. during trajectory tracking, the new estimate can be used for fine-tuning and plausibility within a combined estimation strategy, and the current trajectory tracking interventions can be adapted. The method presented here is based on information about lateral tyre force  $F_y$  and the self-aligning torque  $M_z$ . We introduce the information of  $M_z$ , since self-aligning torque comes into non-linear region earlier than lateral tyre force saturates, as a result, only moderate excitation is needed to estimate road conditions [29]. Besides, total aligning torque (including self-aligning torque information) can be obtained either by steer-by-wire or series production vehicles with Electric Power Steering (EPS) or Active Steering system. Related approaches presented in the literature using these information show several shortcomings. First, observers' stability or convergence problem cannot be well addressed. For example, in [23], a non-linear observer is designed which is only guaranteed to be stable when the front wheel slip angle  $\alpha_f$  and the tyre-road friction coefficient  $\mu_{\max}$  are both over- or underestimated. Ahn proposes a recursive non-linear least squares method in [21], where the global minimum depends highly on the initial guess of  $\mu_{\max}$  and  $\alpha_f$ , which are usually not known very accurately. Moreover, he also proposes a non-linear robust observer in [22]. However, the observer is proven to be locally stable, and the attraction domain cannot cover the whole working area of the tyres. In [24], an Extended Kalman Filter (EKF) to estimate the  $\mu_{\max}$  and  $\alpha_f$  is applied which cannot ensure the stability of the system. Second, no reliable criteria of excitation detection to trigger the update of  $\mu_{\max}$  estimation result are given. As we know, under different road conditions the corresponding lateral acceleration as criteria to indicate the tyres coming into non-linear region is different, for instance, on high friction road condition, lateral acceleration smaller than  $4 \text{ m/s}^2$  is an indication that the tyres still work in the linear region [30] while this value can be much smaller under low friction road conditions. Grip uses yaw rate and derivative of lateral velocity to check the excitation of vehicle lateral dynamics [31]. Similar methods are implemented to detect vehicle excitation [32,33]. However, these criteria cannot be well adapted due to lack of road condition information. Besides, in order to avoid misoperation of ESC, the strategy about when to estimate road condition is conservative, which means some situations suitable for road friction estimation are ignored since there are no excitation criteria uniformly to road

conditions. Hence, the criteria should be proposed to detect excitation regardless of road condition.

Therefore, the two main objectives of this paper are as follows: first, an algorithm is introduced for the problem of road friction coefficient estimation using lateral dynamics. In contrast to EKF and other methods, a proof of asymptotic stability is given with a large attraction domain. In this way, it is ensured that for all possible driver's steering inputs over some excitation level, the estimation result will converge to the real value under nominal system if some proposed assumptions<sup>1</sup> are satisfied. This is important for a subsequent application of the road condition information that requires a reliable input value, e.g. as in the case of trajectory tracking. Second, criteria applicable for all road conditions to detect excitation and decide when to update estimated road friction result are designed. In order to fulfil these objectives, we propose a new framework to estimate road friction coefficient with stability and robustness guarantee. To be more specific, we first adopt a novel strategy to estimate front axle lateral force whose estimation quality is better than classical unknown input observer (UIO) [34]. Then, combined with an indirect measurement based on estimated total aligning torque and front axle lateral force, a non-linear adaptive observer is designed to estimate road friction coefficient with stability guarantee. To increase the robustness of the road friction estimation result, criteria are proposed to decide when to update the estimated road conditions. Simulations and experiments under various road conditions validate the proposed framework and demonstrate its advantage in stability by comparing it with method utilising the widespread EKF. It has to be mentioned that the whole framework is applied under no tractive or braking actions during steering. Compared with authors' previous work [25], substantial improvement is conducted, since in previous work only a classical UIO was applied and the proposed adaptive observer was based on a convex optimisation which needed more computational effort. In addition, no experiments were conducted for validation. In this article, all these shortcomings are addressed.

The main contribution of this paper is as follows.

The relationship between derivative of front axle and rear axle lateral force is analysed by simulation, based on the analytical result an optimised estimation strategy for front axle lateral force is proposed.

A non-linear adaptive observer with stability guarantee is proposed to estimate road friction coefficient based on obtained total aligning torque and estimated front axle lateral force.

The criteria are proposed to detect lateral dynamics excitation and decide when to update estimated road conditions robustly.

The remainder of the study is organised as follows. In Section 2, vehicle and tyre model are introduced. In Section 3, front axle lateral force is estimated based on a novel strategy. In Section 4, a non-linear adaptive observer for road friction estimation is proposed and proved. In Section 5, some discussion is conducted about criteria to update road friction estimation result, meanwhile, the overall estimation framework is demonstrated. In Section 6, simulations and experiments under different road conditions are conducted and the results compared with EKF are illustrated. Finally, conclusion is made in Section 7.

## 2. Vehicle and tyre model

### 2.1. Vehicle model

A non-linear single track model shown in Figure 1 is used to express the lateral dynamics of the vehicle. It considers lateral load transfer and assumes  $\mu_{\max}$  to be piecewise constant, and can be written as

$$\dot{\omega} = \frac{l_f F_{yf} \cos \delta}{I_z} - \frac{l_r F_{yr}}{I_z}, \quad (1a)$$

$$\dot{\beta} = \frac{a_y}{v_x} - \omega, \quad (1b)$$

where  $l_f$  is the distance between the front axle to the centre of gravity,  $l_r$  the distance between the rear axle to the centre of gravity,  $\delta$  the front wheel steering angle,  $F_{yf}$  the front axle lateral force,  $F_{yr}$  the rear axle lateral force,  $v_x$  the slow varying or constant longitudinal velocity,  $\omega$  the yaw rate,  $\beta$  the side slip angle,  $a_y$  the lateral acceleration and  $I_z$  the moment of inertia of the vehicle.

### 2.2. Tyre model

Two related tyre models are used. For  $F_y$ , ‘TMsimple’ is implemented due to its simplicity [35]. For  $M_z$ , the tyre model ‘TMeasy’ is used [36]. These models describe  $F_y$  and  $M_z$  as functions of wheel slip angle  $\alpha$  and road friction  $\mu_{\max}$ :

$$\begin{aligned} F_y &= -K\mu_{\max} \sin[B(1 - e^{-|\alpha|}/A\mu_{\max})] \text{sign}(\alpha) \\ M_z &= F_y \cdot n \end{aligned} \quad (2)$$

and term  $n$  is computed using

$$\begin{cases} \frac{n}{L} = \left(\frac{n}{L}\right)_0 [(1-w)(1-|s|) + w(1-(3-2|s|)s^2)] & \left|\frac{\alpha}{\mu_{\max}}\right| \leq s_y^0 \\ \frac{n}{L} = \left(\frac{n}{L}\right)_0 \left[-(1-w)(|s|-1) \left(\frac{1-w|s|}{1-w}\right)^2\right] & s_y^0 < \left|\frac{\alpha}{\mu_{\max}}\right| \leq s_y^E \\ \frac{n}{L} = 0 & \left|\frac{\alpha}{\mu_{\max}}\right| > s_y^E, \end{cases} \quad (3)$$

where  $K = Y_{\max}$ ,  $B = \pi - \arcsin(Y_{\infty}/Y_{\max})$  ( $Y_{\infty} \leq Y_{\max}$ ) and  $A = (1/dY_0)KB$  which are all constant and only determined by normal force  $F_z$  (see Figure 2);  $L$  denotes the tyre

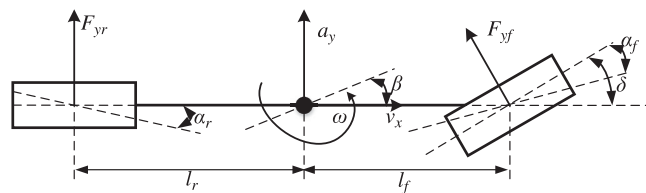


**Figure 1.** Single track model.

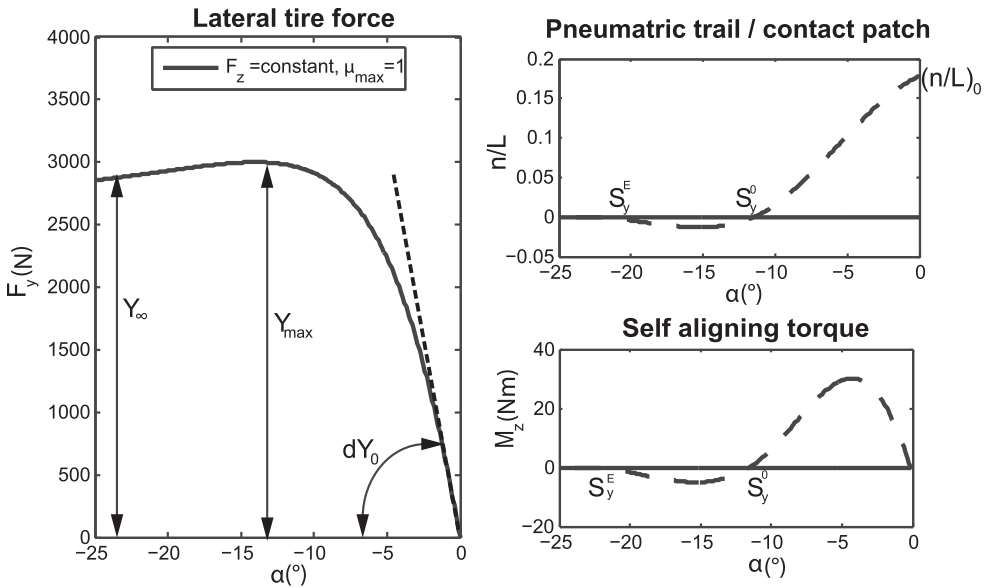


**Figure 2.** Example of a passenger car tyre characteristics under constant normal force and road condition.

road contact length,  $n$  the pneumatic trail,  $(n/L)_0$  the initial value of the pneumatic trail divided by the contact length,  $s = \alpha/(s_y^0 \mu_{\max})$ ,  $w = s_y^0/s_y^E$ , and  $s_y^0$  and  $s_y^E$  are both constant independent of  $\mu_{\max}$  and are identified using experimental data. It has to be mentioned that, in real application, for simplicity we set  $n/L = 0$  when  $|\alpha/\mu_{\max}| > s_y^0$  holds. However,  $s_y^E$  is still important, since it determines  $w$  in  $n/L$  when  $|\alpha/\mu_{\max}| \leq s_y^0$ .

Define  $x = \alpha/\mu_{\max}$ , (2) can be written as

$$\begin{aligned} F_y &= \mu_{\max} \cdot f(x) \\ M_z &= \mu_{\max} \cdot g(x), \end{aligned} \quad (4)$$

which decouples  $x$  and  $\mu_{\max}$  in the expression of  $F_y$  and  $M_z$ . Then tyre characteristics in Figure 3 are obtained under a constant normal force with new abscissa  $x$ . In Figure 3 (right), it can be deduced that the peak of  $M_z$  is at the same value of  $x = x_o$  independent of  $\mu_{\max}$ . In addition, the smaller  $|x|$  is, the closer the relationship of  $|x|$  to  $M_z$  is to a linear one, making a possible estimation of  $\mu_{\max}$  in this area less accurate. In this article,  $|x| \leq x_c$  is used to indicate the quasi-linear region. In this way, we can detect the excitation of lateral dynamics by checking whether the value of  $x$  is pushed into the non-linear region of self-aligning torque regardless of the road conditions. Although the values of  $x$  for the peak and the end of the linear region differ, this assumption for the linear region also holds for  $F_y$  over  $x$ . For different tyre normal forces, the values of  $x_c$  and  $x_o$  vary, however, if we assume the longitudinal velocity changes slowly or is a constant, leading to negligible longitudinal load transfer, both  $x_c$  and  $x_o$  vary little for the overall front lateral force and self-aligning torque in the front axle (especially for low road friction coefficient) and can be assumed constant for this application [38].

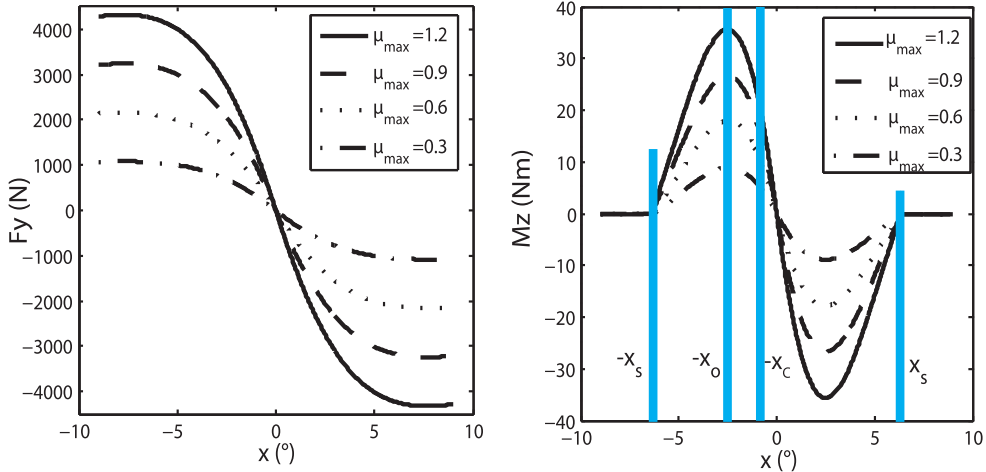


**Figure 3.**  $F_y$  and  $M_z$  varies with  $x$  in different  $\mu_{\max}$  for a constant normal force on [37].

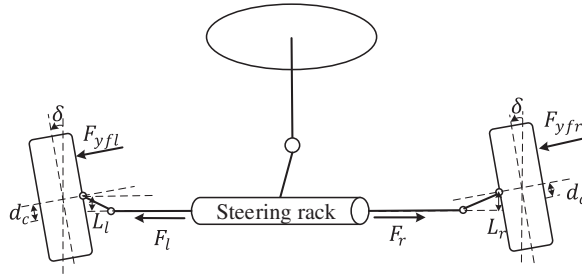


**Figure 4.** Steering system.

### 2.3. Steering system

Usually, the steering system shown in Figure 4 can be written by

$$\begin{cases} \tau_g(t) = F_l(t) * L_l(\delta) - F_r(t) * L_r(\delta) \\ J_s \ddot{\delta} + k_s \dot{\delta} = \tau_g(t) - \tau_{zf}(t), \end{cases} \quad (5)$$

based on [22], where  $J_s$  is the rotational inertia coefficient,  $k_s$  the damping coefficient,  $\delta$  the steering wheel angle,  $\tau_{zf}(t)$  the total aligning torque,  $F_l(t)$  the tie rod force on the left side,  $F_r(t)$  the tie rod force on the right side,  $L_l(\delta)$  and  $L_r(\delta)$  are the distances between the steering rack to the Kingpin separately which vary with steering angle,  $\tau_g(t)$  the aligning torque caused by  $F_l(t)$  and  $F_r(t)$ . It has to be mentioned that in our work both  $F_l(t)$  and  $F_r(t)$  are measured by strain gauge sensors. For vehicles with EPS or active steering system,  $\tau_g(t)$  can also be obtained without extra strain gauge sensor installed in tie rod [21]. Then,  $\tau_{zf}(t)$  can be obtained by an UIO [22] or directly using numerical differential since the wheel steering angle  $\delta$  is quite smooth. Finally, with  $\tau_{zf}$ , a relationship for  $M_{zf}$  and the front lateral forces can be given by

$$\tau_{zf} = M_{zf} + (F_{yfl} + F_{yfr})d_c, \quad (6)$$

where  $F_{yfl}$  is the front left lateral force,  $F_{yfr}$  the front right lateral force,  $d_c$  the mechanical trail of front tyres which is assumed to be the same both front left and right tyres, and  $M_{zf}$  the front axle self-aligning torque.

## 2.4. Model transformation

According to (1b),  $\alpha_f = \beta + l_f \omega / v_x - \delta$  as well as  $F_{yr} = ma_y - F_{yf} \cos \delta$ , we have the following equation:

$$\dot{\alpha}_f = c_1(t)F_{yf} + c_2(t), \quad (7)$$

where  $c_1(t) = (a - b)(\cos \delta) > 0$ ,  $c_2(t) = bma_y - \omega - \dot{\delta}$ ,  $a = 1/mv_x + l_f^2/I_z v_x$ ,  $b = 1/mv_x - l_f l_r / I_z v_x$ ,  $m$  the vehicle mass. For a more detailed deduction of (7), readers can refer to [25].

Applying the result from (4) to the vehicle front axle and considering the lateral load transfer, we have

$$\begin{aligned} F_{yf} &= \mu_{\max} \cdot f_f(x_f, t) \\ M_{zf} &= \mu_{\max} \cdot g_f(x_f, t), \end{aligned} \quad (8)$$

where  $x_f = \alpha_f / \mu_{\max}$ ,  $f_f(x_f, t) := f_{fl}(x_f, t) + f_{fr}(x_f, t)$ ,  $g_f(x_f, t) := g_{fl}(x_f, t) + g_{fr}(x_f, t)$ ,  $f_l$  and  $f_r$  denote front left and front right, respectively.

According to (8), (7) is finally transformed to

$$\begin{aligned} \dot{x}_f &= c_1(t)f_f(x_f, t) + c_2(t)\theta \\ \dot{\theta} &= 0, \end{aligned} \quad (9)$$

where  $\theta = 1/\mu_{\max}$ .

## 3. Front axle lateral force estimation

According to (1a) and combined with  $F_{yr} = ma_y - F_{yf} \cos \delta$ , we obtain

$$\begin{aligned} \dot{\omega} &= \frac{lF_{yf} \cos \delta}{I_z} - \frac{l_r m a_y}{I_z} \\ \dot{F}_{yf} &= p_1(t), \end{aligned} \quad (10)$$

where  $a_y$  is the lateral acceleration and  $p_1(t)$  the derivative of  $F_{yf}$ .

Usually, for estimating  $F_{yf}$ , with classical UIO we have

$$\begin{aligned} \dot{\hat{\omega}} &= \frac{l\hat{F}_{yf} \cos \delta}{I_z} - \frac{l_r m a_y}{I_z} + k_1(\omega - \hat{\omega}) \\ \dot{\hat{F}}_{yf} &= k_2(\omega - \hat{\omega}), \end{aligned} \quad (11)$$

where  $k_1$  and  $k_2$  are the positive constants.

Then, the corresponding error dynamics is

$$\begin{aligned}\dot{\tilde{\omega}} &= \frac{l\tilde{F}_{yf} \cos \delta}{I_z} - k_1 \tilde{\omega} \\ \dot{\tilde{F}}_{yf} &= -k_2 \tilde{\omega} + p_1(t).\end{aligned}\quad (12)$$

Therefore, the steady-state estimation error of  $F_{yf}$  is

$$\tilde{F}_{yf} = \frac{k_1 I_z p_1(t)}{l k_2 \cos \delta}. \quad (13)$$

Since  $k_2$  cannot be set infinite large due to yaw rate measurement noise, we introduce a novel strategy to reduce the estimation error of the front axle lateral force without changing UIO gains, which is

$$\hat{F}_{yf,ave} = \frac{\hat{F}_{yf} + (m a_y - \hat{F}_{yr}) / \cos \delta}{2}, \quad (14)$$

where  $\hat{F}_{yr}$  is the estimated rear axle lateral force, which is observed in a similar way with UIO based on (1a) and  $F_{yf} \cos \delta = m a_y - F_{yr}$ . The corresponding steady-state estimation error of  $F_{yr}$  is

$$\tilde{F}_{yr} = -\frac{k_3 I_z p_2(t)}{l k_4}, \quad (15)$$

where  $k_3$  is a positive constant while  $k_4$  is a negative constant,  $p_2(t)$  the derivative of rear axle lateral force.

The corresponding steady-state estimation error is

$$\begin{aligned}\tilde{F}_{yf,ave} &= F_{yf} - \hat{F}_{yf,ave} \\ &= F_{yf} - \frac{\hat{F}_{yf} + (F_{yf} \cos \delta + F_{yr} - \hat{F}_{yr}) / \cos \delta}{2} \\ &= \frac{F_{yf} - \hat{F}_{yf}}{2} - \frac{F_{yr} - \hat{F}_{yr}}{2 \cos \delta} \\ &= \frac{I_z}{2 l \cos \delta} \left( \frac{k_1 p_1(t)}{k_2} + \frac{k_3 p_2(t)}{k_4} \right).\end{aligned}\quad (16)$$

Comparing (16) and (14), we have

$$\frac{|\tilde{F}_{yf,ave}|}{|\tilde{F}_{yf}|} = \frac{\left| 1 + \frac{k_2 k_3}{k_1 k_4} \frac{p_2(t)}{p_1(t)} \right|}{2}. \quad (17)$$

For this application, we set  $(k_2 k_3) / (k_1 k_4)$  to be  $-1$  to guarantee similar performance of UIOs for front axle and rear axle lateral force estimation. Therefore, as long as  $-1 \leq p_2(t)/p_1(t) \leq 3$ , we can guarantee  $|\tilde{F}_{yf,ave}| \leq |\tilde{F}_{yf}|$ .

In the following, we will use simulation to demonstrate that  $-1 \leq p_2(t)/p_1(t) \leq 3$  holds most of the time with classical manoeuvres. Before conducting simulation, we introduce an evaluation criteria  $p_v$  which demonstrates ratio of time when  $p_2(t)/p_1(t)$  is within  $-1$  and  $3$

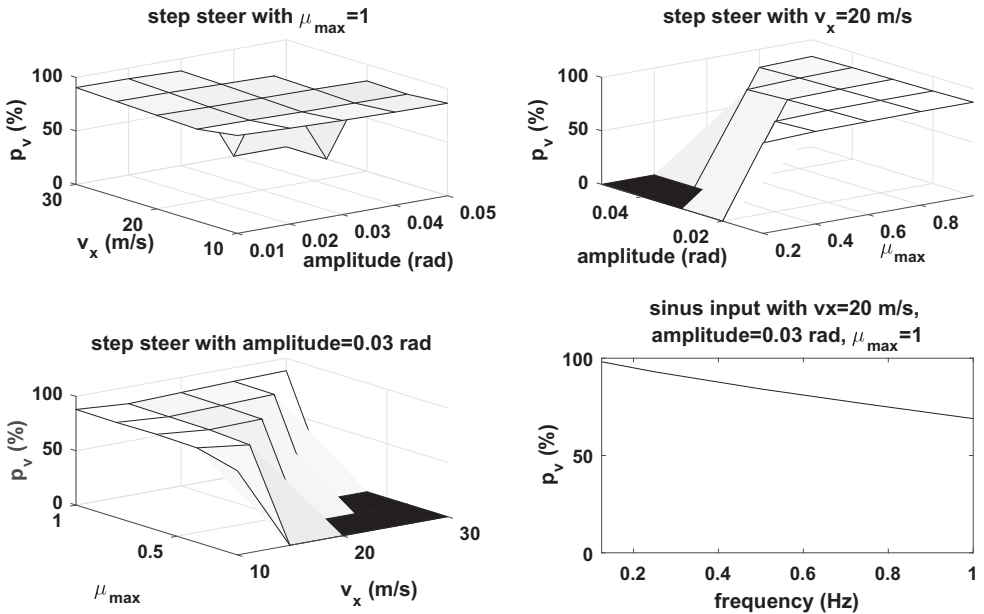


**Figure 5.** Characteristics of  $p_v$  with respect to input space variables at step steer and sinusoidal manoeuvres are simulated.  $p_v$  means the ratio of time when the proposed  $F_{yf}$  estimation strategy being better than classical UIO to overall time in each simulation. Here only surface surrounded by line segments without intersecting with plane  $p_v = 0$  is valid, since other parts are too aggressive to be simulated.

to overall simulation time during one simulation. The manoeuvres chosen for simulations are step steer, sinusoidal input as well as double lane change. The dimensions of the input space for different manoeuvres are various, for instance, there are three input variables for step steer and four for sinusoidal manoeuvre, which are longitudinal velocity  $v_x$ , steer wheel amplitude as well as maximum road friction coefficient  $\mu_{\max}$  (common for both manoeuvres) and steer frequency (additional for sinusoidal manoeuvre). On the contrary, the dimensions of the input space for double lane change are two ( $v_x$  and  $\mu_{\max}$ ).

After the background description, the simulation investigation is conducted. For simplifying simulation effort in step steer, we fix one of these variables ( $v_x$ , steer wheel amplitude and  $\mu_{\max}$ ) each time and study the relationship between  $p_v$  and the rest two. The chosen fixed values are  $\mu_{\max} = 1$ ,  $v_x = 20$  m/s, amplitude = 0.03 rad which are carefully selected, since with this combination the maximum lateral acceleration is around  $4 \text{ m/s}^2$  which is recommended by normal step steer test [39]. The duration time starts from the execution of step steer and ends with recovery of stability (5% of variation around steady yaw rate) of the vehicle. The results can be seen in Figure 5. It has to be mentioned that only surface surrounded by line segments without intersecting with plane  $p_v = 0$  is valid, since other parts are too aggressive to be simulated, which also holds for sinusoidal and double lane change manoeuvres. In Figure 5, we can conclude that  $p_v$  apparently exceeds 50% and is actually larger than 80% which means  $-1 \leq p_2(t)/p_1(t) \leq 3$  holds in most of the simulation time. In a next step, sinusoidal inputs are considered. Since during the transient process of step steer the behaviour of the vehicle is close to that of a vehicle at sinusoidal manoeuvre, we focus on frequency influence here as shown in right down side of Figure 5. As we can see,

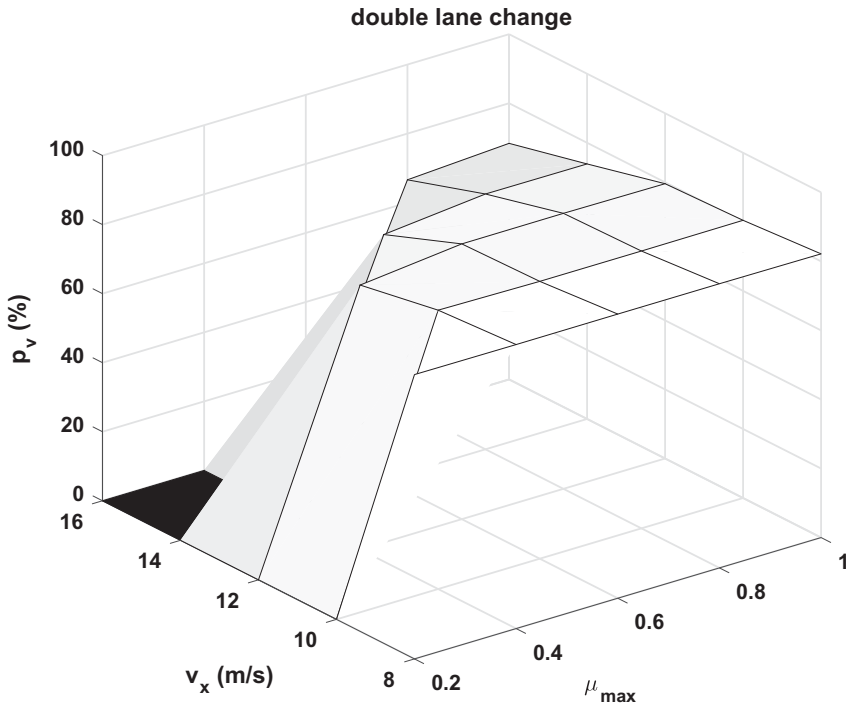


**Figure 6.** Characteristics of  $p_v$  with respect to input space variables at double lane change manoeuvre are simulated.  $p_v$  means the ratio of time when the proposed  $F_{yf}$  estimation strategy being better than classical UIO to overall time in each simulation. Here only surface surrounded by line segments without intersecting with plane  $p_v = 0$  is valid, since other parts are too aggressive to be simulated.

the higher the frequency is, the lower  $p_v$  is, but still much larger than 50%. Finally we simulate double lane change manoeuvre. As illustrated in Figure 6, with increasing of  $v_x$ ,  $p_v$  drops for fixed  $\mu_{\max}$ , while  $p_v$  is robust to  $\mu_{\max}$  when  $v_x$  is fixed. Overall speaking, based on  $p_v$  analysis with simulation, we can demonstrate that our strategy works better than classical UIO for front axle lateral force estimation in most of the time.

In order to more intuitively demonstrate  $F_{yf}$  estimation quality of our novel estimation strategy, we show some exemplary comparison between our proposed strategy and classical UIO considering road condition and velocity as well as steer wheel amplitude variation. Three different manoeuvres – sinusoidal, step steer and double lane change – are performed and the results are illustrated in Figure 7. As can be seen, the estimated results  $\hat{F}_{yf,ave}$  with proposed estimation strategy are better than  $\hat{F}_{yf,nor}$  with classical UIO most of the time in all three manoeuvres regardless of predefined variation, which also verifies the  $p_v$  simulation analysis.

## 4. Non-linear adaptive observer for road friction estimation

### 4.1. Non-linear adaptive observer design

After estimating the front axle lateral force and total aligning torque, we have

$$\hat{F}_{yf,ave} = \mu_{\max} \cdot f_f(x_f, t)$$

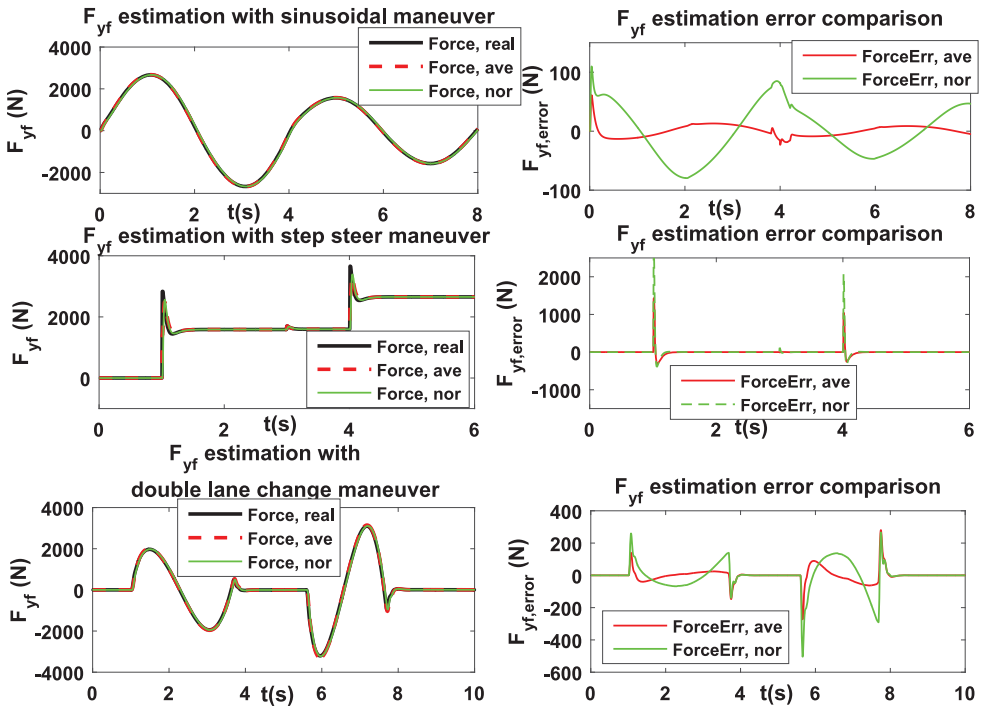


**Figure 7.** Three different manoeuvres – sinusoidal, step steer and double lane change – are demonstrated. Sinusoidal manoeuvre is conducted from high friction with  $v_x = 20 \text{ m/s}$  to low friction road condition (variation happens in the 4th second) with  $v_x = 15 \text{ m/s}$ . Step steer manoeuvre is carried out from low friction to high friction road condition (variation happens in the 3rd second):  $v_x = 15 \text{ m/s}$ . Under low friction road condition, the wheel steering angle jumps from 0 to 0.03 rad and then from 0.03 to 0.05 rad under high friction road condition. Double lane change manoeuvre is performed from low friction to high friction road condition (variation happens in the 4th second):  $v_x = 12 \text{ m/s}$ . Estimation results with postfix 'ave' and 'nor' are based on proposed  $F_{yf}$  estimation strategy and classical UIO estimation, separately.

$$\tau_{zf} = \mu_{\max} \cdot (g_f(x_f, t) + f_f(x_f, t)d_c). \quad (18)$$

In authors' previous work [25], we use convex optimisation to solve  $x_f$  online which needs significant calculation effort. To avoid complex optimisation, we introduce an indirect measurement demonstrated in the following:

$$y(x_f, t) = \left( \frac{f_f(x_f, t)}{g_f(x_f, t) + f_f(x_f, t)d_c} - m_v \right) \text{sign}(x_f) = \left( \frac{\hat{F}_{yf,ave}}{\tau_{zf}} - m_v \right) \text{sign}(-\hat{F}_{yf,ave}), \quad (19)$$

where  $m_v = \lim_{x_f \rightarrow 0} f_f(x_f, t)/(g_f(x_f, t) + f_f(x_f, t)d_c)$  and  $y(x_f, t)$  is a monotonic non-decreasing odd function with respect to  $x_f$  and uniformly to  $t$  (see Figure 8). However, the indirect measurement  $y(x_f, t)$  is confronted with singularity problem when  $\tau_{zf}$  is close to zero, so some processing need to be conducted to improve the  $y(x_f, t)$  quality and can

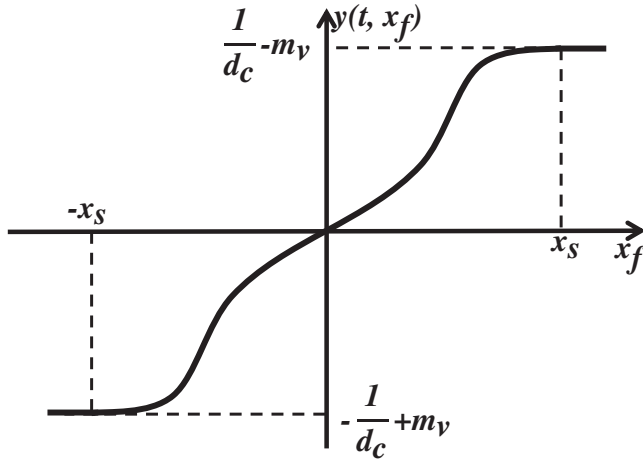


**Figure 8.** Indirect measurement  $y(x_f, t)$  with respect to  $x_f$ . Between  $-x_s$  and  $x_s$  (as shown in Figure 3),  $y(x_f, t)$  is monotonic increasing odd function, otherwise it is constant.

be described as follows:

```

if  $|\hat{F}_{yf,ave}| \leq F_{yf,threshold}$   $\mid |\tau_{zf}| \leq \tau_{threshold} \mid \text{sign}(\tau_{zf} - \hat{F}_{yf,ave} \times d_c) \neq \text{sign}(\hat{F}_{yf,ave})$ 
 $\mid |\hat{F}_{yf,ave}| < |\tau_{zf} \times m_v|$ 
 $y = 0, k_a = 0, k_b = 0;$ 
else
 $y = y(x_f, t); k_a = k_a; k_b = k_b(t);$ 
end

```

where  $\tau_{threshold}$ ,  $F_{yf,threshold}$  are thresholds to judge whether the estimated total aligning torque and front axle lateral force are close to zero or not.  $\text{sign}(\tau_{zf} - \hat{F}_{yf,ave} \times d_c) \neq \text{sign}(\hat{F}_{yf,ave})$  is to detect whether the front axle self-aligning torque and the front axle lateral force have the same sign. Theoretically speaking, they should be the same, but when both of the estimated values are close to zero in the application, the sign may differ. For  $|\hat{F}_{yf,ave}| < |\tau_{zf} \times m_v|$ , if this rule is not respected, there is no solution in the tyre model. If one of the proposed condition is satisfied, we set  $y(x_f, t) = 0, k_a = 0, k_b = 0$ , where  $k_a$  and  $k_b$  are gains for the non-linear adaptive observer and will be described in the following.

Based on this indirect measurement and the model given in (9), we consider the following system:

$$\begin{aligned} \dot{x}_f &= c_1(t)f_f(x_f, t) + c_2(t)\theta \\ \dot{\theta} &= 0 \\ y &= y(x_f, t), \end{aligned} \tag{20}$$

where  $x_f \in \Theta_1 \subset \mathbb{R}$ ,  $\Theta_1 = \{x_f \in \mathbb{R} \mid -x_s \leq x_f \leq x_s\}$ ,  $x_s$  is constant as shown in Figure 3 and  $\theta \in \Theta_2 \subset \mathbb{R}$ ,  $\Theta_1$  and  $\Theta_2$  are compact sets.

The corresponding observer is

$$\begin{aligned}\dot{\hat{x}}_f &= c_1(t)f_f(\hat{x}_f, t) + c_2(t)\hat{\theta} + k_a(y - y(\hat{x}_f, t)) \\ \dot{\hat{\theta}} &= k_b(t)\frac{\partial y(\hat{x}_f, t)}{\hat{x}_f}c_2(t)(y - y(\hat{x}_f, t)),\end{aligned}\quad (21)$$

where  $k_a$  is a positive constant, while  $k_b(t)$  is  $k_c/\max(|c_2(t)|, \epsilon)$  with  $k_c$  and  $\epsilon$  both being positive constant, such that the convergent rate of  $\hat{\theta}$  to the real  $\theta$  will be less influenced by time varying  $c_2(t)$ . Then, the corresponding error dynamics is

$$\begin{aligned}\dot{\tilde{x}}_f &= c_1(t)(f_f(x_f, t) - f_f(\hat{x}_f, t)) + c_2(t)(\theta - \hat{\theta}) - k_a(y - y(\hat{x}_f, t)) \\ \dot{\tilde{\theta}} &= -k_b(t)\frac{\partial y(\hat{x}_f, t)}{\hat{x}_f}c_2(t)(y - y(\hat{x}_f, t)),\end{aligned}\quad (22)$$

where  $\tilde{x}_f = x_f - \hat{x}_f$  and  $\tilde{\theta} = \theta - \hat{\theta}$ .

## 4.2. Stability analysis

At first, the following assumptions and properties will be described.

**Assumption 4.1:** For all  $(t, x_f, \hat{x}_f, \tilde{x}_f) \in \mathbb{R}_{\geq 0} \times \Theta_1 \times \mathbb{R} \times (\Theta_1 - \mathbb{R})$ ,

$$k_{y,low}\tilde{x}_f \leq \tilde{y}(\tilde{x}_f, t), \quad (23)$$

where  $k_{y,low}$  is a positive constant and  $\tilde{y}(\tilde{x}_f, t) = y(x_f, t) - y(\hat{x}_f, t)$ .

**Assumption 4.2:** Suppose that there exists positive scales  $T_1, \epsilon_1$  and  $\epsilon_2$ , such that, for all  $t \in R_{\geq 0}$ , we have

$$\epsilon_1 \leq \int_t^{t+T_1} c_2^2(\tau) d\tau \leq \epsilon_2, \quad (24)$$

with  $c_2(t), \dot{c}_2(t) \in L_\infty$ .

**Property 4.1:** Suppose that Assumption 4.1 holds, then for all  $(t, x_f, \hat{x}_f, \tilde{x}_f) \in \mathbb{R}_{\geq 0} \times \Theta_1 \times \mathbb{R} \times (\Theta_1 - \mathbb{R})$ , we have

$$k_{y,low}\tilde{x}_f \leq \tilde{y}(\tilde{x}_f, t) \leq k_{y,upp}\tilde{x}_f \quad (25)$$

and

$$||f_f(x_f) - f_f(\hat{x}_f)|| \leq k_f ||\tilde{x}_f||, \quad (26)$$

where  $k_{y,upp}$  and  $k_f$  are positive constants.

**Property 4.2:** Suppose that Assumption 4.2 holds, and that  $c_2(t)$  and  $\dot{c}_2(t) \in L_\infty$ , then we have

$$\rho_1 \leq k_b(t) \leq \rho_2 \quad (27)$$

and

$$0 \leq ||\dot{k}_b(t)|| \leq \rho_3, \quad (28)$$

where  $\rho_1$  and  $\rho_2$  as well as  $\rho_3$  are positive constants.

**Property 4.3:** For all  $(t, x_f, \hat{x}_f, \tilde{x}_f) \in \mathbb{R}_{\geq 0} \times \Theta_1 \times \mathbb{R} \times (\Theta_1 - \mathbb{R})$ ,

$$||d_1(t, \tilde{x}_f)|| \leq l_1 ||\tilde{x}_f||^2, \quad (29)$$

where  $l_1$  is a positive constant,  $d_1(t, \tilde{x}_f) = 2k_b(t)(y(x_f, t) - y(\hat{x}_f, t))((\partial y(x_f, t)/\partial x_f - \partial y(\hat{x}_f, t)/\partial \hat{x}_f)\dot{x}_f + (\partial y(x_f, t)/\partial t - \partial y(\hat{x}_f, t)/\partial t)) + \dot{k}_b(t)(y(x_f, t) - y(\hat{x}_f, t))^2$ .

**Theorem 4.1.** Suppose that assumptions 1–2 hold, then there exist positive constant  $k_a$  and bounded positive  $k_b(t)$ , such that if  $k_a$  is large enough, then  $\tilde{x}_f \rightarrow 0, \tilde{\theta} \rightarrow 0$  as  $t \rightarrow \infty$  for  $(\tilde{x}_f, \tilde{\theta}) \in (\Theta_1 - \mathbb{R}) \times (\Theta_2 - \mathbb{R})$ .

**Proof:** Now, the Lyapunov function is defined by

$$V(\tilde{x}_f, t) = k_b(t)(y(x_f, t) - y(\hat{x}_f, t))^2 + \tilde{\theta}^2.$$

Denote the vector  $[\tilde{x}_f; \tilde{\theta}]$  by  $X$  and according to property 1, we have

$$\min(\rho_1 k_{y,low}^2, 1)X^2 \leq V(\tilde{x}_f, t) \leq \max(\rho_2 k_{y,upp}^2, 1)X^2, \quad (30)$$

which indicates that  $V(\tilde{x}_f, t)$  is radially unbounded. Subsequently, we have

$$\begin{aligned} \dot{V} &= 2k_b(t)(y(x_f, t) - y(\hat{x}_f, t)) \left( \frac{\partial y(x_f, t)}{\partial x_f} \dot{x}_f - \frac{\partial y(\hat{x}_f, t)}{\partial \hat{x}_f} \dot{\hat{x}}_f + \frac{\partial y(x_f, t)}{\partial t} - \frac{\partial y(\hat{x}_f, t)}{\partial t} \right) \\ &\quad + 2\tilde{\theta}\dot{\tilde{\theta}} + \dot{k}_b(t)(y(x_f, t) - y(\hat{x}_f, t))^2 \\ &= 2k_b(t)(y(x_f, t) - y(\hat{x}_f, t)) \\ &\quad \left( \left( \frac{\partial y(x_f, t)}{\partial x_f} - \frac{\partial y(\hat{x}_f, t)}{\partial \hat{x}_f} \right) \dot{x}_f + \frac{\partial y(\hat{x}_f, t)}{\partial \hat{x}_f} \dot{\hat{x}}_f + \left( \frac{\partial y(x_f, t)}{\partial t} - \frac{\partial y(\hat{x}_f, t)}{\partial t} \right) \right) \\ &\quad + 2\tilde{\theta}\dot{\tilde{\theta}} + \dot{k}_b(t)(y(x_f, t) - y(\hat{x}_f, t))^2 \\ &= 2k_b(t)(y(x_f, t) - y(\hat{x}_f, t)) \frac{\partial y(\hat{x}_f, t)}{\partial \hat{x}_f} \left( c_1(t)(f_f(x_f) - f_f(\hat{x}_f)) + c_2(t)(\theta - \hat{\theta}) \right. \\ &\quad \left. - k_a(y - y(\hat{x}_f, t)) \right) + 2\tilde{\theta}\dot{\tilde{\theta}} + d_1(t, \tilde{x}_f) \\ &= 2k_b(t)(y(x_f, t) - y(\hat{x}_f, t)) \frac{\partial y(\hat{x}_f, t)}{\partial \hat{x}_f} \left( c_1(t)(f_f(x_f) - f_f(\hat{x}_f)) - k_a(y - y(\hat{x}_f, t)) \right) \\ &\quad + 2k_b(t)(y(x_f, t) - y(\hat{x}_f, t)) \frac{\partial y(\hat{x}_f, t)}{\partial \hat{x}_f} c_2(t)\tilde{\theta} \\ &\quad + 2\tilde{\theta} \left( -k_b(t) \frac{\partial y(\hat{x}_f, t)}{\partial \hat{x}_f} c_2(t)(y - y(\hat{x}_f, t)) \right) + d_1(t, \tilde{x}_f) \\ &\leq -2k_a k_b(t) \frac{\partial y(\hat{x}_f, t)}{\partial \hat{x}_f} (y(x_f, t) - y(\hat{x}_f, t))^2 + 2k_b(t)c_1(t)k_{y,upp}^2 k_f ||\tilde{x}_f||^2 + l_1 ||\tilde{x}_f||^2 \\ &\leq (-2k_a \rho_1 k_{y,low}^3 + 2\rho_2 c_1(t)k_{y,upp}^2 k_f + l_1) ||\tilde{x}_f||^2. \end{aligned} \quad (31)$$

Since  $c_1(t)$  is positive and bounded, then if  $k_a$  is chosen large enough, there exists a positive constant  $k^*$ , such that

$$\dot{V}(X, t) \leq -k^* \|\tilde{x}_f\|^2. \quad (32)$$

According to Theorem 8.4 Barbalat lemma in [40], it can be deduced that

$$\tilde{x}_f \rightarrow 0 \quad \text{as} \quad t \rightarrow \infty.$$

Combined with Assumption 4.2 and applying Corollary 4.3.1 from [41], we can reason out that

$$\tilde{\theta} \rightarrow 0 \quad \text{as} \quad t \rightarrow \infty.$$

■

## 5. Criteria and overall estimation framework description

### 5.1. Criteria description

To detect vehicle lateral excitation, reliable criteria which are robust to road conditions and meanwhile not conservative to utilise excitation are important. The criteria in this study consist of two parts. The first and also the most important one is to compare estimated  $|x_f|$  with a defined constant threshold  $x_{f,c}$  shown in Figure 3 (shown as  $x_c$ ) which is applicable for all road conditions and thus can be used to detect excitation effectively. Moreover, this threshold is the boundary between quasi-linear region and non-linear region of front axle self-aligning torque, therefore, the decision of when to estimate road friction is not conservative due to sufficient usage of tyre non-linearity. The second part is an auxiliary criterion to alleviate the misuse of the first criterion. When vehicle lateral dynamic excitation is too small, the tyre characteristics remain exactly in linear region, which leads to singular estimation of  $x_f$ . As a result, the estimated  $x_f$  may be much larger than the real value and thus leads to misuse of the criterion one. Therefore, we introduce extra criteria to alleviate its misoperation. To be more specific, the activation of criterion one is based on the precondition that the estimated total aligning torque, the measured lateral acceleration and the estimated front axle lateral force are simultaneously larger than their corresponding defined thresholds, which increases the robustness of  $\mu_{max}$  estimation. These criteria are shown more detailed with mathematical description as follows:

```

if  $|\hat{x}_f| > x_{f,c}$  &  $|\tau_{zf}| > \tau_{threshold}$  &  $|a_y| > a_{y,threshold}$  &  $|\hat{F}_{yf,ave}| > F_{yf,threshold}$ 
     $\hat{\mu}_{max} = \mu_{max,update};$ 
else
     $\hat{\mu}_{max} = \mu_{max,pre};$ 
end

```

where  $\tau_{threshold}$ ,  $F_{yf,threshold}$  as well as  $a_{y,threshold}$  are thresholds to avoid updating road conditions when the excitation is too small,  $\hat{\mu}_{max}$  is the final estimated road condition,  $\mu_{max,update}$  is the road friction estimation result from observer,  $\mu_{max,pre}$  is value of  $\hat{\mu}_{max}$  in previous step. It has to be mentioned that  $\tau_{threshold}$  and  $F_{yf,threshold}$  here are the same values for avoiding singularity in the indirect measurement  $y(x_f, t)$ .

## 5.2. Overall estimation framework (AVE)

For better understanding of the whole description in this article, the overall estimation framework is presented (see Figure 9). All parts of this estimation framework are further referred as AVE. We first utilise the measurements (yaw rate, lateral acceleration as well as longitudinal velocity, etc.) to estimate the front axle lateral force with a novel strategy based on UIO. Meanwhile, the front axle total aligning torque is estimated on the basis of measured tie rod force. Then, regarding the front axle lateral force and total aligning torque as input, an indirect measurement  $y(x_f, t)$  based on some selection criteria is generated. Combining with this indirect measurement, a non-linear adaptive observer is designed to

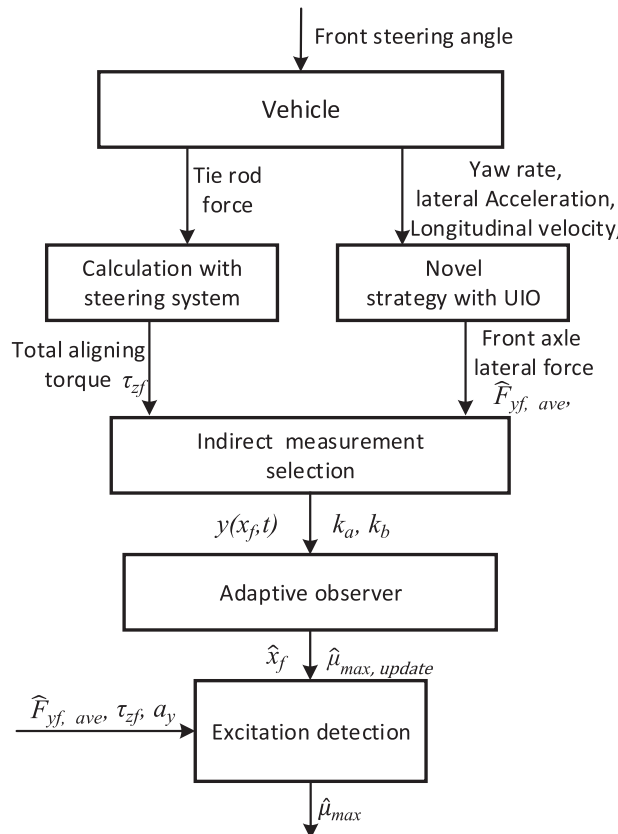


**Figure 9.** Overall estimation framework, which is further referred to as AVE.

**Table 1.** Basic information of AVE and EKF.

	AVE	EKF
State equations	$\begin{cases} \dot{x}_f = c_1(t)f_f(x_f, t) + c_2(t)\theta \\ \dot{\theta} = 0 \end{cases}$	$\begin{cases} \dot{\alpha}_f = aF_{yf} + bF_{yr} - w - \dot{\delta} \\ \dot{\mu}_{max} = 0 \end{cases}$
Measurements	$m a_y, \tau_{zf} \rightarrow y(x_f, t)$	$m a_y, \tau_{zf}$
States illustrated in figures	$x_f, \frac{1}{\theta}$	$\frac{\alpha_f}{\mu_{max}}, \mu_{max}$

**Table 2.** Gains and thresholds in the criteria for AVE in the simulations and experiments.

	Simulation	Experiment
Gains	$k_a = 1$ $k_b(t) = \frac{k_c}{\max( c_2(t) , \epsilon)},$ where $k_c = 0.25, \epsilon = 0.02$	$k_a = 0.3$ $k_b(t) = \frac{k_c}{\max( c_2(t) , \epsilon)},$ where $k_c = 0.03, \epsilon = 0.25$
Thresholds in the criteria	$x_{f,c} = 0.01 \text{ rad}$ $\tau_{threshold} = 35 \text{ Nm}$ $a_{y,threshold} = 1 \text{ m/s}^2$ $F_{yf,threshold} = 900 \text{ N}$	$x_{f,c} = 0.02 \text{ rad}$ $\tau_{threshold} = 40 \text{ Nm}$ $a_{y,threshold} = 1 \text{ m/s}^2$ $F_{yf,threshold} = 900 \text{ N}$

**Table 3.** Settings for EKF in simulations and experiments.

	Simulation	Experiment
Covariance of the process noise	$Q = [0.00053; 0; 0, 0.3]$	$Q = [0.003; 0; 0, 0.3]$
Covariance of the observation noise	$R = [10,000; 0; 0, 50]$	$R = [90,000; 0; 0, 400]$
Condition for freezing $\mu_{max}$ estimation	$ a_y  \leq 1 \text{ m/s}^2$ or $ \tau_{zf}  \leq 35 \text{ Nm}$	$ a_y  \leq 1 \text{ m/s}^2$ or $ \tau_{zf}  \leq 40 \text{ Nm}$

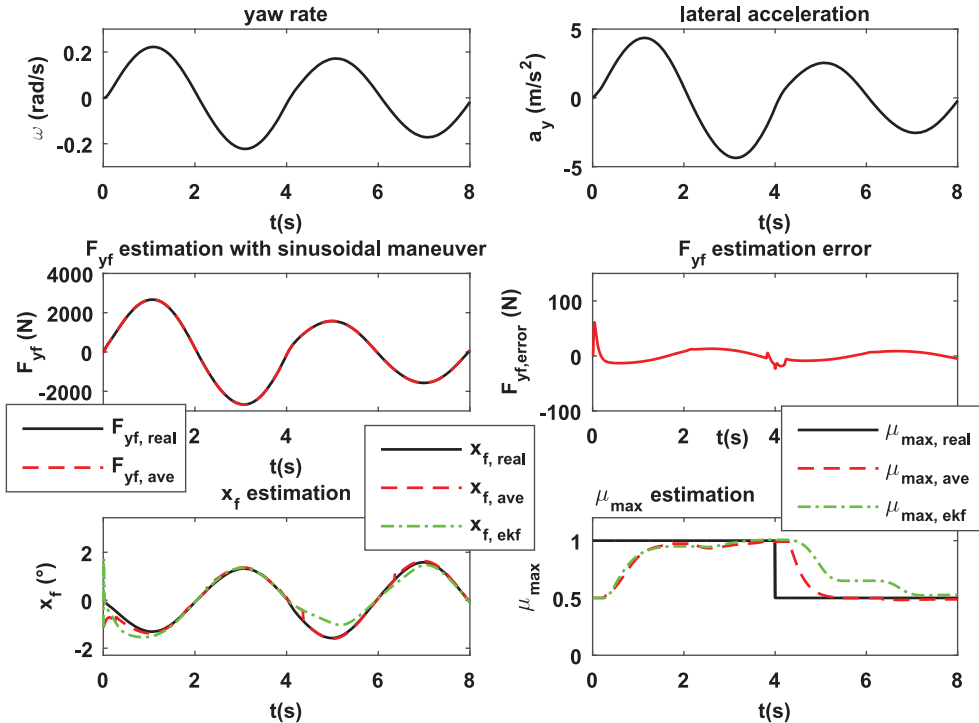


**Figure 10.** Sinusoidal manoeuvre from high friction ( $v_x = 20 \text{ m/s}$ ) to low friction road condition ( $v_x = 15 \text{ m/s}$ ): wheel steering angle amplitude is  $0.03 \text{ rad}$ , frequency is  $0.25 \text{ Hz}$ . Estimation results with postfix 'ave' and 'ekf' are based on the proposed method and EKF, separately.

estimate the road friction coefficient. To increase the robustness of the estimation result, an excitation detection block is proposed with carefully defined criteria to better update estimated road friction coefficient.

## 6. Simulation and experiment results

### 6.1. Simulation results of the front axle lateral force and the road friction estimation

In this part, based on a non-linear single track model (considering lateral road transfer), three different manoeuvres – sinusoidal, step steer and double lane change – are simulated to show estimation results of the front axle lateral force,  $\hat{x}_f$  as well as the road friction coefficient. In addition, the estimated road friction result from the proposed observer framework (AVE) are compared to the results from a method based on [24] using an EKF.<sup>2</sup> The basic information of the two methods is listed in Table 1. It can be noticed that though the state variables used for estimation are different in AVE and EKF, the states illustrated in figures (both in simulations and experiments) are the same<sup>3</sup> for a better comparability. The gains and criteria of AVE, and settings of EKF for both simulations and experiments are listed in Tables 2 and 3, respectively. The conditions for freezing  $\mu_{\max}$  estimation in EKF are added in Table 3, which are used to freeze  $\mu_{\max}$  estimation result during inferior observability. Besides, it has to be mentioned that the adaptation of the gains and thresholds in Table 2 is possible to be conducted quite fast for different platforms of vehicles<sup>4</sup> with different tyre settings (winter or summer tires). This is because the vehicle

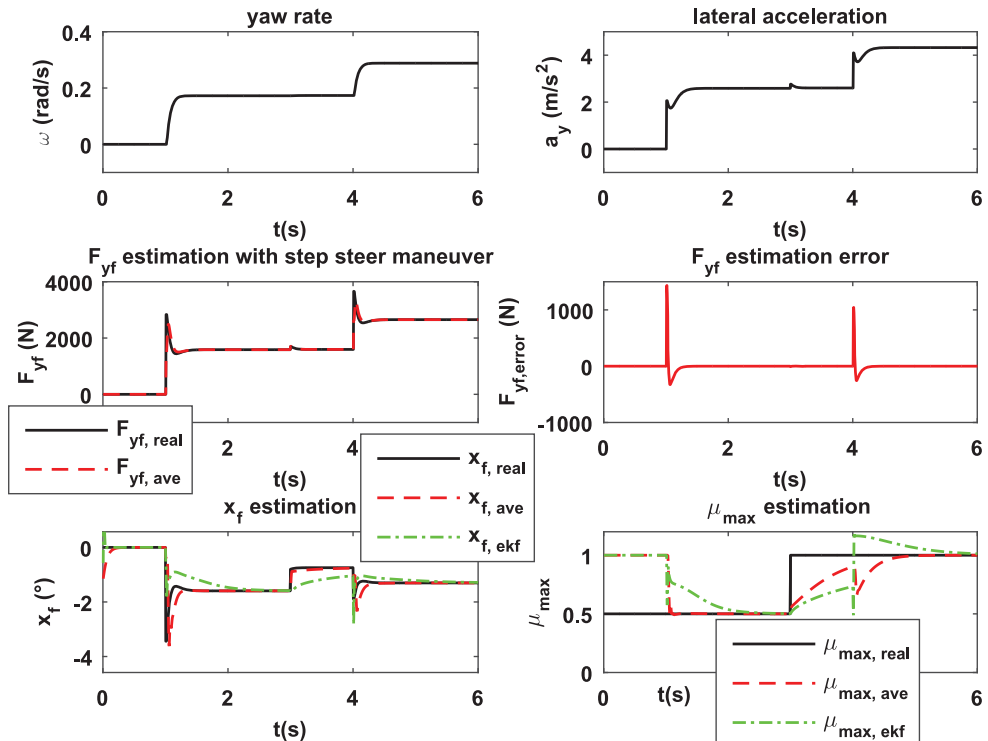


**Figure 11.** Step steer manoeuvre from low friction to high friction road condition:  $v_x = 15 \text{ m/s}$ . Under low friction road condition, the wheel steering angle jumps from 0 to 0.03 rad and then from 0.03 rad to 0.05 rad under high friction road condition. Estimation results with postfix 'ave' and 'ekf' are based on the proposed method and EKF, separately.

parameters and noise level of measurements in different platforms will usually not differ by 1 order of magnitude, and hence, as long as one pair of gains and thresholds in the criteria are well tuned for one platform, fine adjustments will be enough for other platforms in application.

The simulation results about three different manoeuvres are illustrated in Figure 10, Figure 11 as well as Figure 12, separately. As can be seen, in AVE, the front axle lateral force can be estimated well in sinusoidal and double lane change manoeuvres. In the step steer manoeuvre,  $\hat{F}_{yf,ave}$  is observed with small delay at first due to sudden jump of steering angle and then converge to the real values. Regarding  $\mu_{max}$  and  $x_f$  estimation, results from AVE are overall better than those from EKF. In sinusoidal and step steer manoeuvres,  $\mu_{max}$  and  $x_f$  estimation results from AVE can converge faster and be more accurate than those from EKF. In double lane change manoeuvre,  $\mu_{max,ave}$  and  $x_{f,ave}$  are observed well while  $\mu_{max,ekf}$  and  $x_{f,ekf}$  diverge between 1 and 8 s. It can be noticed that the  $\mu_{max,ave}$  is not updated until some excitation level is reached in Figure 10 (around the 4th second) and Figure 12 (between 4 and 5.5 seconds), though during these time the real road condition changes in both manoeuvres. This is partly contributed by road friction excitation detection block,<sup>5</sup> where we formulate the criteria (described in Section 5.1) for guaranteeing robust road friction estimation result.

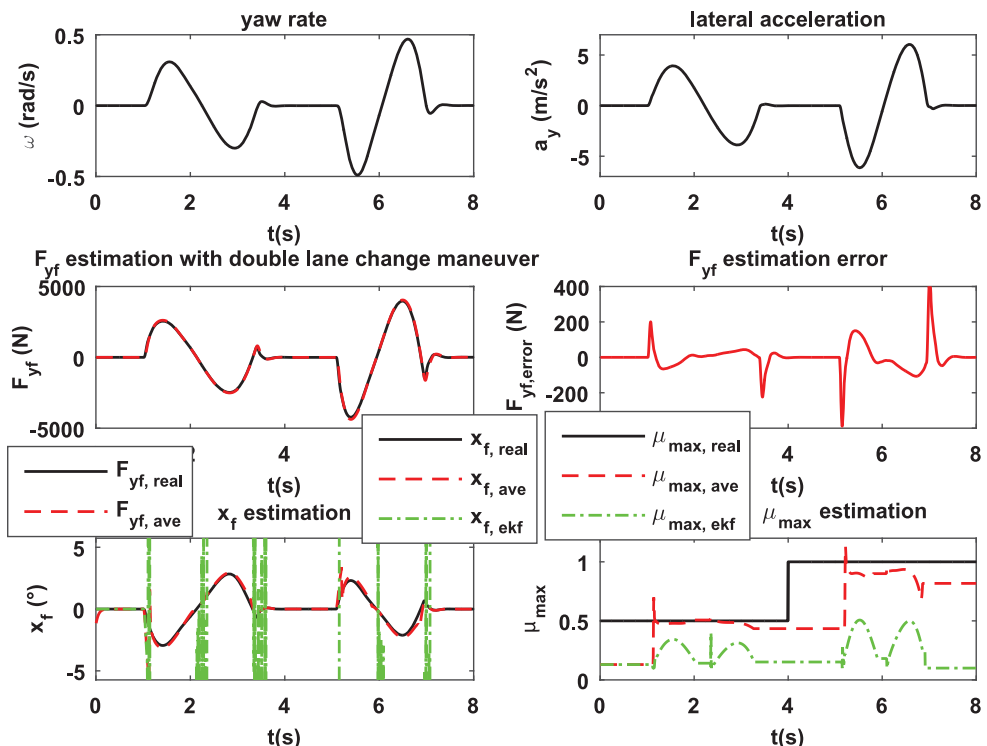


**Figure 12.** Double lane change manoeuvre from low friction to high friction road condition:  $v_x = 13.5$  m/s. Estimation results with postfix 'ave' and 'ekf' are based on the proposed method and EKF, respectively.



**Figure 13.** Test racing car Roding Roadster. © Photo: Thyssenkrupp.

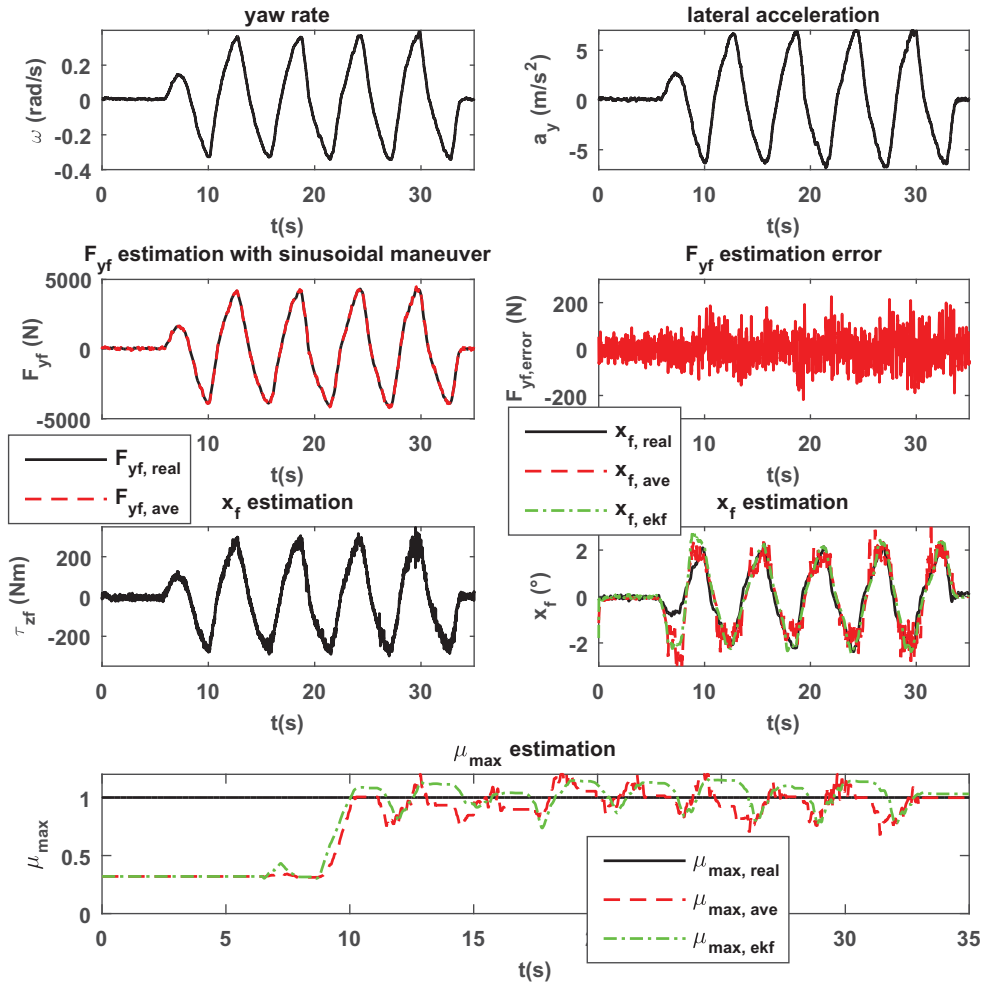


**Figure 14.** Sinusoidal manoeuvre on high friction road condition:  $v_x = 20$  m/s with frequency 0.2 Hz. Estimation results with postfix 'ave' and 'ekf' are based on the proposed method and EKF, separately.

## 6.2. Vehicle test results of front axle lateral force and road friction estimation

The vehicle experiments are conducted both on Nardo Italy (concrete test track) and Sweden (grinded ice test track) with a racing car called Roding Roadster, see Figure 13, with validated vehicle parameters available [42]. The real values of front axle lateral force,  $\mu_{\max}$  as well as  $x_f$  are obtained as follows: for the front axle lateral force, it is represented by  $I_z\dot{\omega} + l_r m_a y/l \cos \delta$  which is deduced from a single track model. The actual friction coefficients are inferred from full brake on the concrete test track and lateral limit handling on the grinded ice test track, respectively. The actual lateral velocity is measured using VBOX speed sensor [43] on concrete test track and is replaced by simulated lateral velocity based on a well-parametrised non-linear single track model<sup>6</sup> (considering lateral road transfer) on the grinded ice test track. Combining the inferred  $\mu_{\max}$  with measured lateral velocity, we obtain  $x_f$ . The rest of the signals applied in the proposed method are

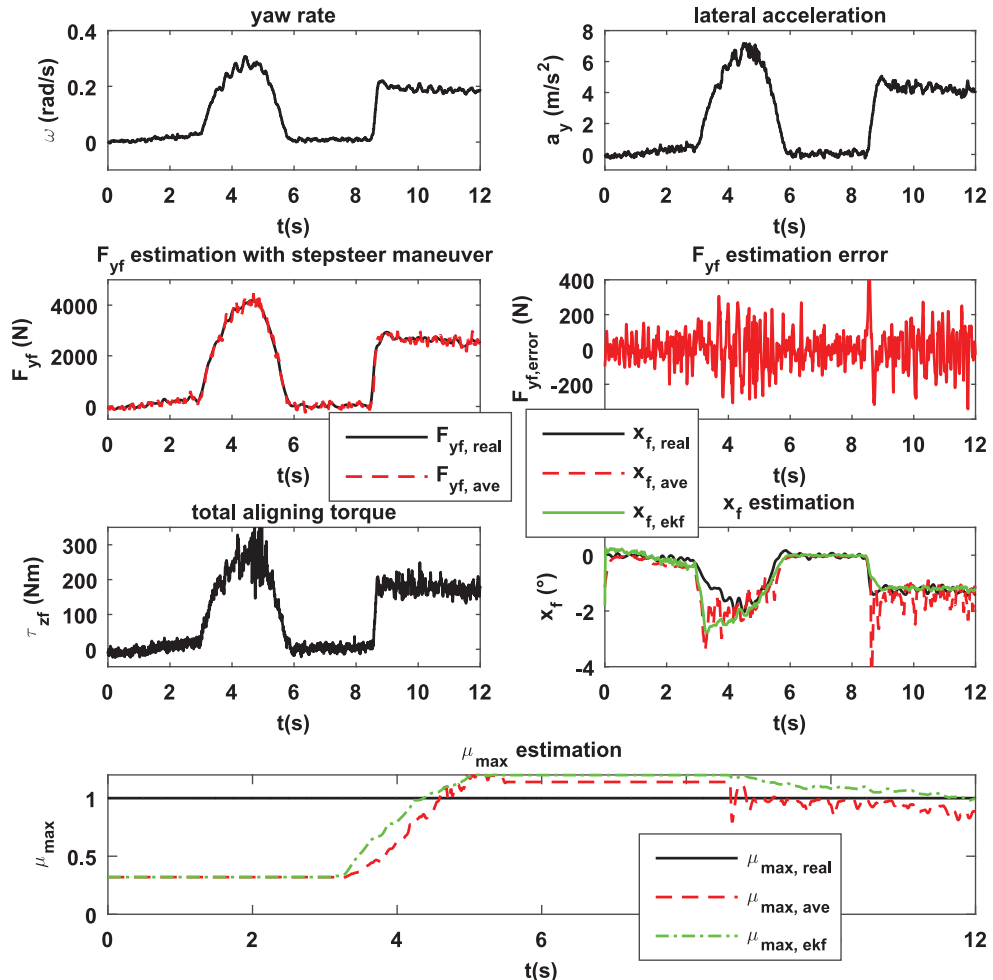


**Figure 15.** Step steer manoeuvre on high friction road condition:  $v_x = 25 \text{ m/s}$ . Estimation results with postfix 'ave' and 'ekf' are based on the proposed method and EKF, separately.

obtained and processed as follows. Signals like lateral acceleration and yaw rate are directly measured. The wheel steering angle of front left and right is obtained based on measured steering wheel angle and a lookup table. The longitudinal velocity is measured by VBOX speed sensor. For the front axle total aligning torque, at first the tie rod forces are measured with strain gauge sensors, then the steering system equations (5) are applied to calculate the total aligning torque. During application, the total aligning torque is low-pass filtered with  $1/0.03s + 1$  to reduce the influence of heavy noise on road friction estimation results. Furthermore, the gains and thresholds in the criteria of AVE, and the settings of EKF for experiments can refer to Table 2 and Table 3, respectively. It can be noticed that the gains for AVE are quite different in simulations and experiments, which are determined based on the balance between estimation convergence rate and sensitivity of estimation results to noise as well as uncertainties. Besides, the covariance of the process and observation noise in EKF for simulations and experiments are decided by considering noise level and model uncertainties.

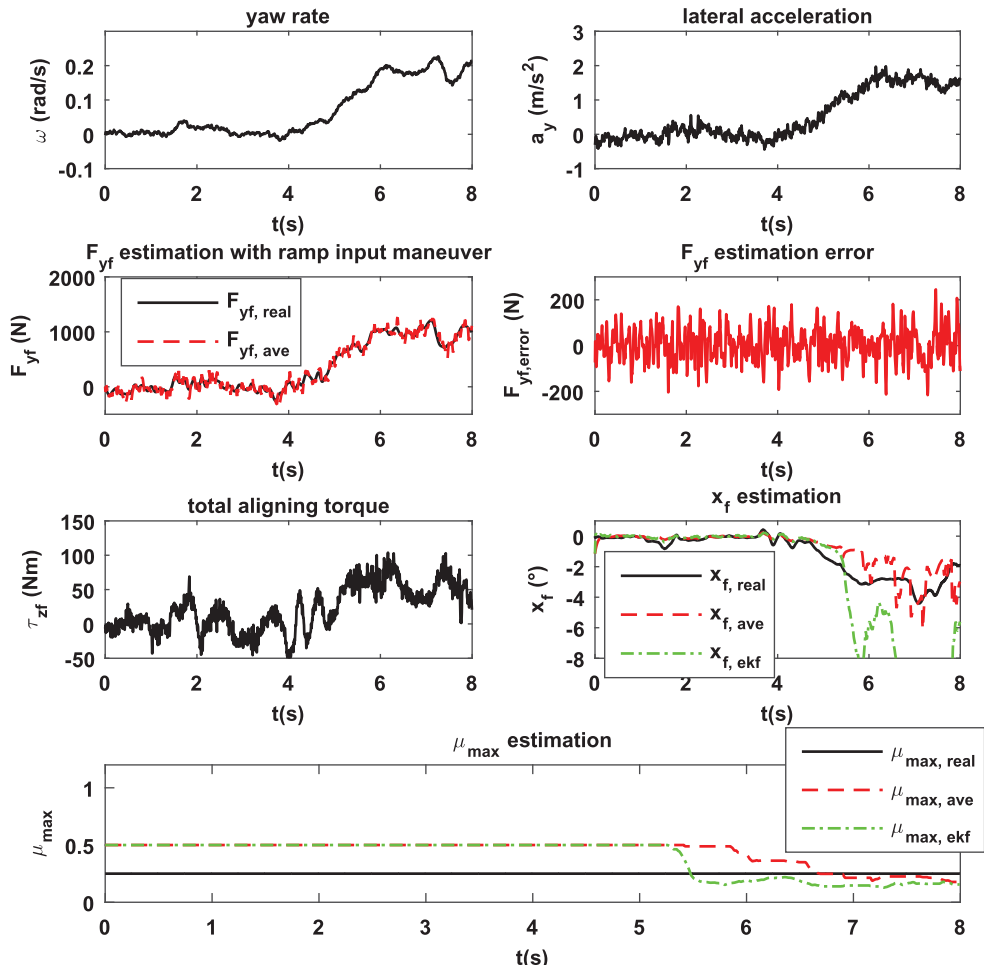


**Figure 16.** Ramp input manoeuvre on low friction road condition:  $v_x = 8.5$  m/s. Estimation results with postfix 'ave' and 'ekf' are based on the proposed method and EKF, separately.

On the concrete test track, Figure 14 demonstrates a sinusoidal manoeuvre with a 0.2 Hz steering input and constant velocity 20 m/s. Figure 15 shows step steer manoeuvre with constant velocity 25 m/s. Both manoeuvres illustrate good estimation results with AVE and EKF. In Figure 14,  $\hat{F}_{yf,ave}$  is estimated accurately with low estimation error.  $\hat{x}_f$  is overestimated both by AVE and EKF at first, then converges to the real one.  $\hat{\mu}_{\max}$  can be estimated accurately both by AVE and EKF with similar convergent rate. In Figure 15, the  $\hat{F}_{yf,ave}$  estimation quality is not as good as that in sinusoidal manoeuvres, especially around the 5th second, because the signal quality of yaw rate and lateral acceleration is worse than that in sinusoidal manoeuvre.  $\hat{x}_f$  increases quite fast from zero to around 3° at first for both AVE and EKF between 0 and 3 s, because the road friction estimation results are frozen this time (for AVE, due to the indirect measurement  $y(x_f, t)$  selection rule, gains  $k_a$  and  $k_b$  are set to

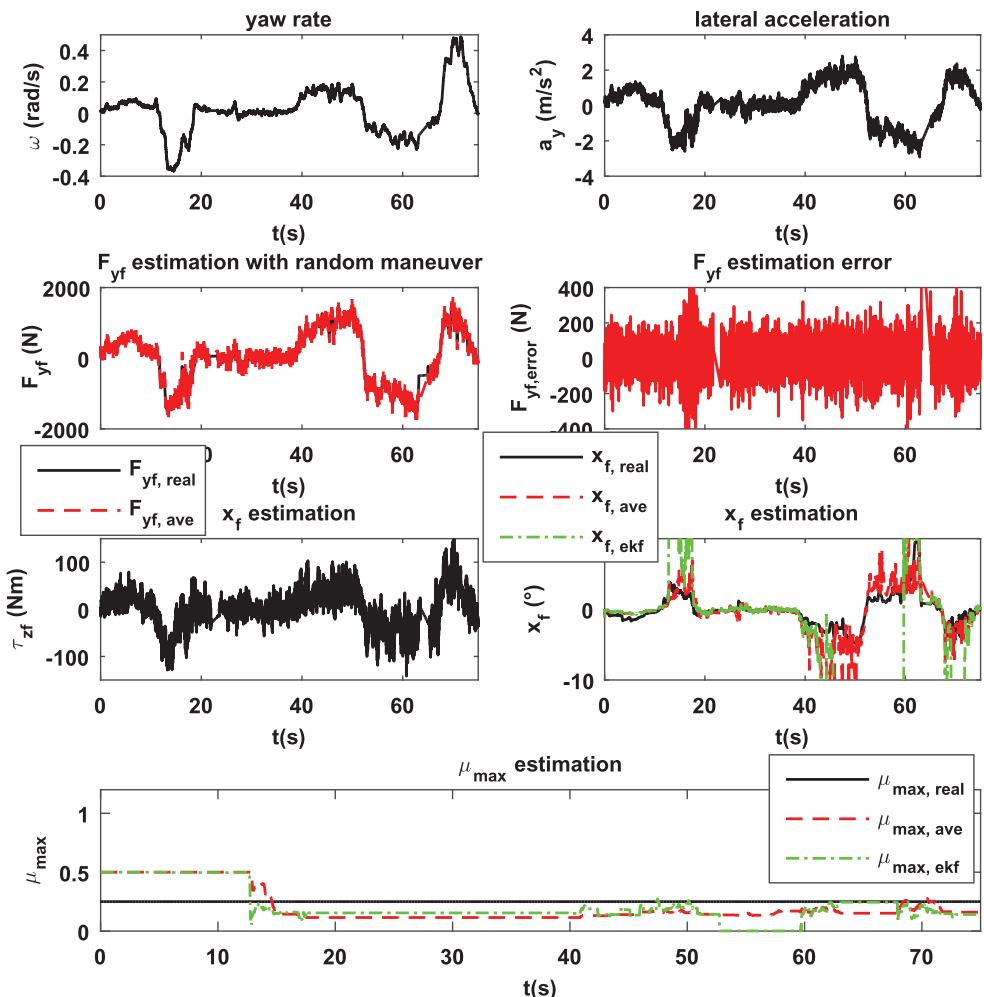


**Figure 17.** Random steering manoeuvre on low friction road condition:  $v_x$  is slow varying around 12 m/s from 0 to 55 s, then changes to 7 m/s and stay around it. Postfix real, ave, ekf refer to real values, estimated results from the proposed method and estimated results from EKF, respectively.

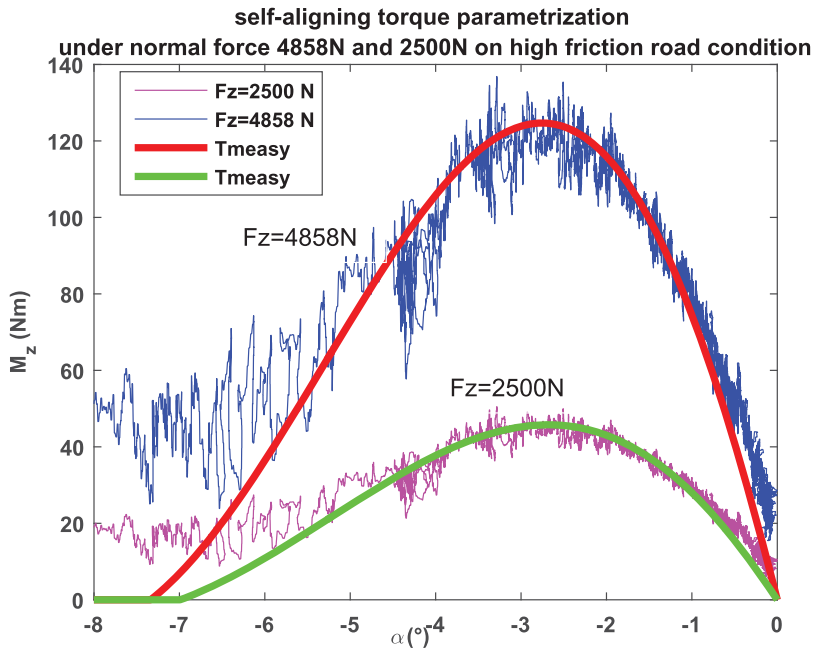


**Figure 18.** Self-aligning torque parametrisation for normal forces 4858 N and 2500 N on road condition  $\mu_{\max} = 1$  with a constant radius (30 m) circular driving manoeuvre.

zero, while for EKF, the conditions for freezing  $\hat{\mu}_{\max}$  are still satisfied) and  $\hat{x}_f$  is thus estimated with underestimated  $\hat{\mu}_{\max}$  in both AVE and EKF. Afterwards, both  $x_{f,ave}$  and  $x_{f,ekf}$  converge to the real value with  $x_{f,ekf}$  illustrating better quality.  $\hat{\mu}_{\max}$  results from AVE and EKF are similar, but results from EKF can converge a little bit faster. The reader may feel confused why we need so large excitation to estimate the road condition on concrete test track, this is because we use a racing car tyre, whose lateral force and self-aligning torque characteristics are linear until quite large excitation, see Figure 18, from which it can be noticed that the value of  $x_f$  with respect to peak point of self-aligning torque is roughly  $2.8^\circ$ . However, in both of these experimental manoeuvres, peak value of  $x_f$  does not reach  $2.8^\circ$ . So, such excitation is necessary for road friction on concrete test track.

On the grinded ice test track, Figure 16 shows a ramp input manoeuvre with longitudinal velocity being around 8.5 m/s, and Figure 17 demonstrates a random steering manoeuvre, in which  $v_x$  is slow varying around 12 m/s from 0 to 55 s and then changes to 7 m/s and stay around it. Both Figure 16 and Figure 17 demonstrate that the estimation errors of  $\hat{F}_{yf,ave}$  are small. Besides,  $\hat{\mu}_{\max}$  is estimated well from AVE in both figures but not from EKF. More specifically, in Figure 16,  $\hat{\mu}_{\max}$  from AVE converges to the real value slower than that from EKF, this is because in AVE, we have an excitation detection block to guarantee robust estimation result. In Figure 17,  $\hat{\mu}_{\max}$  from EKF can also react faster than those from AVE, however, between 52 and 60 s,  $\hat{\mu}_{\max}$  from EKF diverges while that from AVE is still stable.

### 6.3. Summary of the estimation results

In summary, the front axle lateral force can be estimated accurately during the framework of the proposed method (AVE), and with this estimation result, road friction can



be observed well. When there is no measurement noise with nominal system (simulation), AVE can estimate  $\mu_{\max}$  faster and more accurate than EKF does. Meanwhile, AVE can also guarantee stability of the estimation error of  $\mu_{\max}$  while EKF cannot in some manoeuvres. When there is measurement noise with model uncertainties (experiment),  $\mu_{\max}$  estimation results from AVE achieve similar accuracy with those from EKF (in stable situations). However, the results from AVE converge a little bit slower than those from EKF, because in AVE there is also an excitation detection block which aims at outputting robust estimation result and thus the thresholds in which may be set conservative due to noise and model uncertainties. Nevertheless, AVE can always output a stable estimated road friction in the experiments while EKF cannot, which is the biggest advantage of AVE.

## 7. Conclusion

In this study, we present a framework to estimate road friction coefficient with stability and robustness guarantee by using total aligning torque in vehicle front axle during steering. We first utilise both front and rear axle information to estimate front axle lateral force and achieve a better result compared with classical UIO with only front axle information. Then, combined with an indirect measurement based on estimated total aligning torque and front axle lateral force, a non-linear adaptive observer is designed to estimate road friction coefficient with stability guarantee. To increase the robustness of the road friction estimation result, criteria are proposed to decide when to update the estimated road conditions. Simulations and experiments under various road conditions validate the proposed framework and demonstrate its advantage in stability by comparing it with method utilising EKF.

In the future work, an optimised estimation framework will be designed to avoid  $F_{yf}$  estimation, in this way less noise will be introduced and singularity of indirect measurement for non-linear adaptive observer can be eliminated. Hence, a better estimation result of road friction may be obtained.

## Notes

1. These assumptions are listed in the proof section 4.2
2. An EKF is chosen for comparison, because linearisation-based methods (like EKF) are widely used in road friction estimation with lateral dynamics [18,24,44]. In [24], the authors originally did not use  $a_y$  as measurement. For a fair comparison,  $a_y$  is introduced as an extra measurement in the application and the single track model is transformed into a form with  $\alpha_f$  and  $\mu_{\max}$  as state variables.
3.  $x_f = \alpha_f / \mu_{\max}, 1/\theta = \mu_{\max}$
4. B, C, D or E class vehicles, SUVs with two axles and four wheels as well as equipped with EPS or similar systems.
5. The indirect measurement selection block also makes some contribution, since with that the estimation process of road friction will be ceased if some thresholds are not reached.
6. Due to sensor reasons, the lateral velocity cannot be well measured in grinded ice test track, which is however not important, because we only pay attention to road friction coefficient estimation. Furthermore, tyre parameters are already identified by a Test truck in Switzerland (for parameters of  $F_y$ ) and by vehicle test in Nardo Italy (for parameters of  $M_z$ ), separately. Therefore, the only function of the lateral velocity in grinded ice test track is to become a reference value for comparing with estimated  $x_f$ .

## Acknowledgements

The authors express their thanks to colleagues at Thyssenkrupp Presta AG for the conduction of vehicle experiments. This work is supported by China Scholarship Council [grant number 201406260208].

## Disclosure statement

No potential conflict of interest was reported by the authors.

## References

- [1] Wallman C, Aström H. Friction measurement methods and the correlation between road friction and traffic safety: a literature review. Technical report. Linköping, Sweden: Swedish National Road and Transport Research Institute; 2001.
- [2] Samiee S, Shao L, Rogic R, et al. A comprehensive algorithm for automatic emergency lane-change. Proceedings of the 25th International Symposium on Dynamics of Vehicles on Roads and Tracks (IAVSD); 14–18 Aug 2017; Queensland, Australia; 2017.
- [3] Chen C, Jia Y.M., Shu M, et al. Hierarchical adaptive path-tracking control for autonomous vehicles. *IEEE Trans Intell Transp Syst.* 2015;16:2900–2912.
- [4] Uchanski MR. Road friction estimation for automobiles using digital signal processing methods [doctoral dissertation]. Berkeley (CA): University of California; 2001.
- [5] Andersson M, et al. Road friction estimation. Technical report. Saab Automobile AB; 2007.
- [6] Holzmann F, Bellino M, Siegwart R, et al. Predictive estimation of the road–tire friction coefficient. Proceedings of the IEEE International Conference on Control Applications; 4–6 Oct 2006; Munich, Germany; 2006. p. 885–890.
- [7] Sato Y, Kobayash D, Kageyama I, et al. Study on recognition method for road friction condition. Proceedings of the Annual Congress, Society of Automotive Engineers of Japan (JSOE Annual Congress); Yokohama JSOE Convention Proceedings; Japan; 2006. p. 43–06.
- [8] Yamada M, Oshima T, Ueda K, et al. A study of the road surface condition detection technique for deployment on a vehicle. *JSOE Rev.* 2003;24(2):183–188.
- [9] Torbrügge S. Testing and understanding of tire–road interaction on wet roads. Proceedings of the 13th Symposium Reifen und Fahrwerk; Vienna, Austria; 2015.
- [10] Eichhorn U, Roth J. Prediction and monitoring of tyre/road friction. Proceedings of the 24th FISITA Congress; 7–11 Jun 1992; London, England; 1992. p. 67–74.
- [11] Tuononen A. On-board estimation of dynamic tyre forces from optically measured tyre carcass deflections. *Int J Heavy Veh Syst.* 2009;16(3):362–378.
- [12] Alonso J, López J, Pavón I, et al. On-board wet road surface identification using tyre/road noise and support vector machines. *Appl Acoust.* 2014;76:407–415.
- [13] Kongrattanaprasert W, Nomura H, Kamakura T, et al. Application of neural network analysis to automatic detection of road surface conditions utilizing tire noise from vehicles. Proceedings of the 2009 ICCAS-SICE; 18–21 Aug 2009; Fukuoka, Japan; 2009.
- [14] Kongrattanaprasert W, Nomura H, Kamakura T, et al. Detection of road surface states from tire noise using neural network analysis. *IEEJ Trans Ind Appl.* 2010;130(7):920–925.
- [15] Gustafsson F. Slip-based tire–road friction estimation. *Automatica.* 1997;33(6):1087–1099.
- [16] Mueller S, Uchanski M, Hedrick K. Estimation of the maximum tire–road friction coefficient. *J Dyn Sys Meas Control.* 2003;4:607–617.
- [17] Rajamani R, Phanomchoeng G, Piyabongkarn D, et al. Algorithms for real-time estimation of individual wheel tire–road friction coefficients. *IEEE/ASME Trans Mechatron.* 2012;17(6):1183–1195.
- [18] Baffet G, Charara A, Stephan J. Sideslip angle, lateral tire force and road friction estimation in simulations and experiments. Proceedings of the IEEE International Conference on Control Applications; 4–6 Oct 2006; Munich, Germany; 2006. p. 903–908.
- [19] Ding N, Taheri S. Application of recursive least square algorithm on estimation of vehicle sideslip angle and road friction. *Math Problem Eng.* 2010.



- [20] Grip HF, Imsland L., Johansen TA, et al. Nonlinear vehicle side-slip estimation with friction adaptation. *Automatica*. **2008**;44(3):611–622.
- [21] Ahn C, Peng H, Tseng HE. Estimation of road friction for enhanced active safety systems: Algebraic approach. Proceedings of the 2009 American Control Conference (ACC'09); 10–12 Jun 2009; St. Louis, MO; **2009**. p. 1104–1109.
- [22] Ahn C, Peng H, Tseng HE. Robust estimation of road frictional coefficient. *IEEE Trans Control Syst Technol*. **2013**;21:1–13.
- [23] Hsu Y-J, Gerdes JC. The predictive nature of pneumatic trail: tire slip angle and peak force estimation using steering torque. Proceedings of the 9th International Symposium on Advanced Vehicle Control (AVEC'08); 6–9 Oct 2008; Kobe, Japan; **2008**. p. 80–85.
- [24] Matsuda T, Jo S, Nishira H, et al. Instantaneous estimation of road friction based on front tire sat using Kalman filter. *SAE Int J Passeng Cars Mech Syst*. **2013**;6:147–153.
- [25] Shao L, Lex C, Hackl A, et al. Estimation of tire road friction during vehicle steering. Proceedings of the 13th International Symposium on Advanced Vehicle Control (AVEC'16); 13–16 Sept 2016; Munich, Germany; **2016**.
- [26] Koskinen S. Sensor data fusion based estimation of tire road friction to enhance collision avoidance [doctoral dissertation]. Tampere, Finland: The Tampere University of Technology; **2010**.
- [27] Tuononen A, Hartikainen J. Tyre-road friction potential estimation by data fusion. Technical report. Espoo, Finland; Helsinki University of Technology; **2010**.
- [28] Ahn C. Robust estimation of road friction coefficient for vehicle active safety systems [doctoral dissertation]. Ann Arbor (MI): University of Michigan; **2011**.
- [29] Hsu J. Estimation and control of lateral tire forces using steering torque [doctoral dissertation]. Stanford (CA): Stanford University; **2007**.
- [30] Mitschke M, Wallentowitz H. *Dynamik der Kraftfahrzeuge*. Heidelberg: Springer; **2014**.
- [31] Grip HF, Imsland L, Johansen TA, et al. Estimation of road inclination and bank angle in automotive vehicles. Proceedings of the 2009 American Control Conference (ACC'09); 10–12 Jun 2009; St. Louis, MO; **2009**. p. 426–432.
- [32] Fukada Y. Slip-angle estimation for vehicle stability control. *Veh Syst Dyn*. **1999**;32(4–5):375–388.
- [33] Hac A, Simpson M. Estimation of vehicle side slip angle and yaw rate. *SAE Technical Paper*. SAE International; **2000**.
- [34] Radke A, Gao Z. A survey of state and disturbance observers for practitioners. Proceedings of the American Control Conference (ACC'06); 14–16 Jun 2006; Minneapolis, MN; **2006**. p. 5183–5188.
- [35] Hirschberg W. *Fahrzeugdynamik*. Skript. TU Graz, Austria: FTG; **2014**.
- [36] Rill G. *Road vehicle dynamics, fundamentals and modeling*. Boca Raton: Taylor & Francis Group; **2012**.
- [37] Takagi F. An estimation method of the maximum tire road friction coefficient using an electric power assist steering. Proceedings of the 10th International Symposium on Advance Vehicle Control (AVEC'10) 22–26 Aug 2010; Loughborough, UK; **2010**. p. 13–15.
- [38] Shao L, Lex C, Hackl A, et al. Road friction estimation using recursive total least squares. Proceedings of the IEEE Intelligent Vehicle Symposium (IV); 19–22 Jun 2016; Gothenberg, Sweden; **2016**.
- [39] ISO. *Road vehicles – lateral transient response test methods*. ISO 7401, International Organization for Standardization; **1988**.
- [40] Khalil H. *Nonlinear systems*. 3rd ed. London: Pearson; **2001**.
- [41] Ioannou AP, Sun J. *Robust adaptive control*. Upper Saddle River (NJ): Prentice Hall; **1996**.
- [42] Mitterrutzner A. Development and validation of a vehicle model for real time application on a steer-by-wire prototype [Master's thesis]. Graz, Austria: Technical University; **2015**.
- [43] Automotive V. [cited 2018 Feb 04]. Available from: <https://www.vboxautomotive.co.uk/index.php/en/>. VBOX Automotive; **2018**.
- [44] Hsu Y-J, Laws S, Gadda C, et al. A method to estimate the friction coefficient and tire slip angle using steering torque. Proceedings of the ASME 2006 International Mechanical Engineering Congress and Exposition; 5–10 Nov 2006; Chicago, IL; **2006**. p. 515–524.